DENSIFICATION OF DTM GRID DATA USING SINGLE SATELLITE IMAGERY

M.A. Rajabi, J.A.R. Blais

Dept. of Geomatics Eng., University of Calgary, Calgary, AB, T2N 1N4, Canada, – (marajabi, blais)@ucalgary.ca

KEY WORDS: Digital Terrain Model, Shape from Shading, Satellite Imagery, Irradiance Model, Curvature Consistency

ABSTRACT:

Digital Terrain Models (DTMs) are simply regular grids of elevation measurements over the land surface. DTMs are mainly extracted by applying the technique of stereo measurements on images available from photogrammetry and remote sensing. Enormous amounts of local and global DTM data with different specifications are now available. However, there are many geoscience and engineering applications which need denser DTM grid data than available. Fortunately, advanced space technology has provided much single (if not stereo) high-resolution satellite imageries almost worldwide. Nevertheless, in cases where only monocular images are available, reconstruction of the object surfaces becomes more difficult. Shape from Shading (SFS) is one of the methods to derive the geometric information about the objects from the analysis of the monocular images. This paper discusses the use of SFS methods with single high resolution satellite imagery to densify regular grids of heights. Three different methodologies are briefly explained and then implemented with both simulated and real data. Moreover, classification techniques are used to fine tune the albedo coefficient in the irradiance model. Numerical results are briefly discussed.

1. INTRODUCTION

DTMs are used for the analysis of topographical features in GISs and numerous engineering computations as well as scientific applications. Rajabi and Blais [2001] briefly reviewed and referenced a number of sources for DTMs and their applications in both engineering and science.

Stereo measurements from pairs of aerial photographs or satellite images have mainly been used as the primary data in producing DTMs. Information from double or multiple images in overlap areas ensures reliable and stable models for geometric and radiometric processing. Especially recently, with the rapid improvement in remote sensing technology, automated analysis of stereo satellite data has been used to derive DTM data ([Gugan and Dowman, 1988], [Simard et al, 1988], and [Tam, 1990]).

Today, with the need for the better management of the limited natural resources, there are numerous geoscience and engineering applications which require denser DTM data than available. Unfortunately stereo satellite imagery is not available everywhere. Obviously, time and cost are two important factors that often prevent us from field measurements. While interpolation techniques are fast and cheap, they have their own inherent difficulties and problems, especially in terms of accuracy of interpolation in rough terrain.

On the other hand, the availability of single satellite imagery for nearly all of the Earth is taken for granted nowadays. However, reconstruction of objects from monocular images is very difficult, and in some cases, not possible at all. Inverse rendering or the procedure of recovering three-dimensional surfaces of unknown objects from two-dimensional images is an important task in computer vision research. Shape from Shading (SFS) [Horn, 1970] [Horn, 1990], [Zhang et al, 1994] is one of the techniques used for inverse rendering which converts the reflectance characteristics in images to shape information.

This paper discusses the application of SFS techniques to improve the quality of the interpolated DTM grid data with single satellite imagery of better resolution than the DTM data. The idea is highly motivated by the wide availability of satellite remotely sensed imagery such as Landsat TM and SPOT HRV imagery. Section 2 briefly reviews the general SFS problem and the methods implemented in this paper. Section 3 provides numerical tests of the methods explained in Section 2 in more detail. Last but not least, Section 4 provides some concluding remarks.

2. SHAPE FROM SHADING

2.1 Image Formation

SFS is one of the methods which transforms single or stereo 2D images to a 3D scene. Basically, it recovers the surface shape from gradual variations of shading in the image. The recovered shape can be expressed either in terrain height z(x,y) or surface normal **N** or surface gradient $(p,q) = (\partial z / \partial x, \partial z / \partial y)$.

Studying the image formation process is the key step to solve the SFS problem. A Lambertian model is the simplest one in which it is assumed that the grey level at each pixel depends only on light source direction and surface normal. Assuming that the surface is illuminated by a distant point source, we have the following equation for the image intensity:

$$R(x, y) = \rho \ \mathbf{N} . \mathbf{L} = \rho \frac{pl_1 + ql_2 + l_3}{\sqrt{p^2 + q^2 + 1}} \qquad (1)$$

where ρ is the surface albedo, **N** is the normal to the surface and $\mathbf{L} = (l_1, l_2, l_3)$ is the light source direction. Even with known ρ and **L**, the SFS problem will still be a challenging subject, as this is one nonlinear equation with two unknowns for each pixel in the image. Therefore, SFS is intrinsically an

underdetermined problem and in order to get a unique solution, if there is any at all, we need to have some constraints.

Based on the conceptual differences in the algorithms, there are three different strategies to solve the SFS problem [Rajabi and Blais, 2001]: 1. Minimization (regularization) approaches 2. Propagation approaches, and 3. Local approaches. A more detailed survey of SFS methods can be found in [Zhang et al, 1999]. The following subsections very briefly review the minimization approach, which is widely used in to solve the SFS problem, and the other variants of the minimization approach which are used here to enhance the solution.

2.2 Minimization Approach

Based on one of the earliest minimization methods, the SFS problem is formulated as a function of surface gradients, while brightness and smoothness constraints are added to ensure that a unique solution exists [Ikeuchi and Horn, 1981]. The brightness constraint ensures that the reconstructed shape produces the same brightness as the input image. The smoothness constraint in terms of second order surface gradients helps in reconstruction of a smooth surface. Brooks and Horn [1985] defined the error functional:

$$I = \iint ((E(x,y) - \mathbf{N}.\mathbf{L})^2 + $$
$$\lambda(\|\mathbf{N}_x\|^2 + \|\mathbf{N}_y\|^2) + \mu(\|\mathbf{N}\|^2 - 1))dxdy \qquad (2)$$

where E(x,y) is the grey level in the image, $\mathbf{N}_x$ and $\mathbf{N}_y$ are the partial derivatives of the surface normal with respect to x and y directions respectively and the constants λ and μ are Lagrangian multipliers. As it can be seen the functional has three terms: 1) the brightness error which encourages data closeness of the measured images intensity and the reflectance function, 2) the regularizing term which imposes the smoothness on the recovered surface normals, and 3) the normalization constraint on the recovered normals.

The functional is minimized by applying variational calculus and solving the Euler equation: The resulting fixed-point iterative scheme for updating the estimated normal at the location of (i,j) and epoch k+1, using the previously available estimate from epoch k is:

$$\mathbf{N}_{i,j}^{k+1} = \frac{1}{1 + \mu_{i,j}(\varepsilon^2/4\lambda)}\left(\mathbf{M}_{i,j}^k + \frac{\varepsilon^2}{4\lambda}\left(E_{i,j} - \mathbf{N}_{i,j}^k.\mathbf{L}\right).\mathbf{L}\right) \quad (3)$$

where

$$\mathbf{M}_{i,j}^k = \frac{1}{4}(\mathbf{N}_{i+1,j}^k + \mathbf{N}_{i-1,j}^k + \mathbf{N}_{i,j+1}^k + \mathbf{N}_{i,j-1}^k) \qquad (4)$$

There are two comments about this update equation. First, it seems that one has to solve for the Lagrangian multiplier $\mu_{i,j}$ on a pixel-by-pixel basis. However, as it is seen $\mu_{i,j}$ enters the update equation as a multiplying factor which doesn't change the direction of the update normal, therefore we can replace that factor by a normalization step. The second comment is about the geometry of the update equation. As it is seen, the update equation is composed of two components. The first one comes from the smoothness constraint while the second one is a response to the physics of image irradiance equation.

The main disadvantage of the Brook and Horn method or any other similar minimization approach is the tendency of over smoothing the solution resulting in the loss of fine detail. Selecting a conservative value for the Lagrangian multiplier is a very challenging issue in this method. However, in an attempt to overcome this problem, Horn [1990] starts the solution with a large value for the Lagrangian multiplier and reduces the influence of the smoothness constraint in each iterations as the final solution is approached.

2.3 Modified Minimization Approaches

As it was mentioned in the previous section, the update equation is composed of two components, the smoothness part and the data closeness part. As the first attempt to solve the over smoothing problem with the general minimization approach, an adaptive regularization parameter $\lambda(i,j)$ instead of a fixed λ is suggested to be used to adaptively control the smoothness over the image space [Gultekin and Gokmen, 1996]. In each iteration, the space varying regularization parameter at location (i,j) can be determined by the following function:

$$\lambda_{new} = (1 - e^{-\frac{c(i,j)}{V_T}})\lambda_{min} + (e^{-\frac{c(i,j)}{V_T}})\lambda_{old}(i,j) \quad (5)$$

where c(i,j) is the control parameter, V_T is a time constant that regulates the rate of exponential decrease and λ_{min} is a preselected minimum value that $\lambda(i,j)$ may have. The control parameter is defined as c(i,j)=|I(i,j)-R(i,j)|, where |-| denotes the absolute value and the function λ_{new} is an exponentially decreasing function with the following properties:

$$\lim_{c(i,j)\to 0} \lambda_{new} = \lambda_{old}(i,j),$$
$$\lim_{c(i,j)\to\infty} \lambda_{new} = \lambda_{min} \qquad (6)$$

so that the regularization parameter is only allowed to decrease with the iterations.

Another method to solve the over smoothing problem is to use a robust error kernel in conjunction with curvature consistency instead of a quadratic smoothness. The robust regularizer constraint function can be defined as [Worthington and Hancock, 1999]:

$$\rho_\sigma(\|N_x\|) + \rho_\sigma(\|N_y\|) \qquad (7)$$

where $\rho_\sigma(\eta)$ is a robust kernel defined on the residual η and with width parameter σ. Among different robust kernels, it is proved that the sigmodial-derivative M-estimator, a continuous version of Huber's estimator, has the best properties for handling surface discontinuities [Worthington and Hancock, 1999] and is defined by:

$$\rho_\sigma(\eta) = \frac{\sigma}{\pi} \log \cosh\left(\frac{\pi\eta}{\sigma}\right). \tag{8}$$

Applying calculus of variations to the constraint function using the above mentioned kernel results in the corresponding update equation. Here σ, the width parameter of the robust kernel, is computed based on the variance of the shape index. Based on Koenderink and Van Doorn [1992] the shape index is another way of representing curvature information. It is a continuous measure which encodes the same curvature class information as the mean and Gauss curvature, but in an angular representation. In terms of surface normals, the shape index is defined as [Koenderink and Van Doorn, 1992]:

$$\phi = \frac{2}{\pi} \tan^{-1} \frac{\mathbf{N}_{x1} + \mathbf{N}_{y2}}{\sqrt{(\mathbf{N}_{x1} - \mathbf{N}_{y2})^2 + 4\mathbf{N}_{x2}\mathbf{N}_{y1}}} \tag{9}$$

where the second subscripts 1 and 2 correspond to the x and y components respectively. The variance dependence of the kernel in eq. (7) is controlled using the exponential function:

$$\sigma = \sigma_0 \exp\left(-\left(\frac{1}{N}\sum \frac{(\phi_l - \phi_c)^2}{\Delta\phi_d^2}\right)^{1/2}\right) \tag{10}$$

where σ_0 is the reference kernel width which we set to one, ϕ_c is the shape index associated with the central normal of the neighborhood, $\mathbf{N}_{i,j}$, ϕ_l is one of the neighboring shape index values and $\Delta\phi_d$ is the difference in the shape index between the center values of adjacent curvature classes which is equal to 1/8 [Koenderink and Van Doorn, 1992].

The other modification that can be done on the minimization approach is on the data closeness part of the update equation. We know that the set of surface normals at a point which satisfy the image irradiance equation define a cone about the light source direction. In other words, the individual surface normals can only assume directions that fall on this cone. At each iterations the updated normal is free to move away from the cone under the action of the local smoothness. However, we can subsequently map it back onto the closest normal residing on the cone. This has not only numerical stability advantages but also all normal vectors in the intermediate states are solutions of the image of irradiance equation. In other words, the update equation for the surface normals can be written as:

$$\mathbf{N}_{i,j}^{k+1} = R(\theta)\,\mathbf{M}_{i,j}^{k} \tag{11}$$

where

$$\theta = -\cos^{-1}\left(\frac{\mathbf{M}_{i,j}^{k} \cdot \mathbf{L}}{\|\mathbf{M}_{i,j}^{k}\|\|\mathbf{L}\|}\right) + \cos^{-1}\mathbf{E}. \tag{12}$$

$\mathbf{M}_{i,j}^{k}$ in eq. 11 is the surface normal that minimizes the smoothness constraint while $R(\theta)$ is the rotation matrix of angle θ which maps the updated normal to the closest normal lying on the cone of ambiguity (Figure 1). The axis of rotation is found by taking the cross product of the intermediate update with the light source direction:
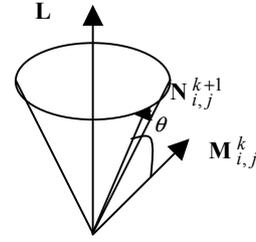

Figure 1. The ambiguity cone. $\mathbf{L}$ is the light source vector, $\mathbf{M}_{i,j}^{k}$ is the surface normal which minimizes the smoothness constraint and $\mathbf{N}_{i,j}^{k+1}$ is the updated surface normal.

3. NUMERICAL TESTS

3.1 Processing Steps

The main goal of this investigation is to improve the accuracy of the interpolated DTM grid data by applying SFS techniques to the corresponding single satellite imagery, while the original DTM data are used as boundary constraints in the SFS problem.

The basic assumption here is that the satellite imagery has one dyadic order better resolution than the original DTM data. We also assume that 1) the surface is Lambertian (which is questionable in reality), 2) the surface albedo is known (by applying classification techniques to multispectral satellite imageries), 3) the surface is illuminated by a distant point source (Sun), and finally 4) the position of the light source is known.

Our approach deals with a patch at a time (Figure 2) with forty nine points. Sixteen grid points have known heights (dark circles) from DTM grid data and the other thirty three are points with the interpolated heights (unmarked grid points). Our main objective is to improve the accuracy of the interpolation for the five innermost unknown points.

The method essentially consists of three stages: 1) preprocessing, 2) processing, and 3) postprocessing. The

preprocessing stage itself has three steps. In the first step, using interpolation (bilinear) techniques, the heights of the unknown points in the patch are estimated. When dealing with the real height data, if there is a gap in height measurements due to any reason (such as existing rivers or lakes), the whole patch is left untouched.

Classification of the image data is the second step of preprocessing stage. The Mahalanobis classifier [Richards, 1986], which is one of the supervised classification methods, is used to classify the image data. The choice of Mahalanobis classifier is because of its simplicity while using the covariance information. After the classification is done, the average grey level data in each class is used to tune the albedo coefficient in irradiance model.
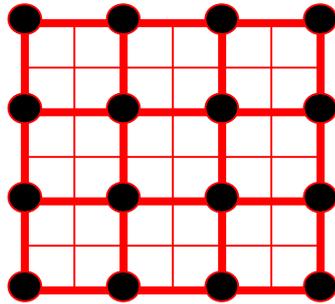

Figure 2. A patch: Circles are the grid points with known heights from DTM grid data and the unmarked ones are the points with the interpolated heights.

In the third step of preprocessing stage, using the known grid points, the relative orientation of the inner most square in the patch with respect to the light source is estimated. If this relative orientation implies that the patch is in the shadow, then there would be no useful shading information to improve the accuracy of the interpolated heights. Therefore, in this case the interpolated heights are considered the final height values.

Otherwise, the processing stage for each patch consists of three steps. In the first step, the smoothed surface normals (based on one of the three methods explained in Section 2 are computed. Then in the second step these surface normals are mapped onto the corresponding ambiguity cones. Finally in the third step, the surface normals are passed to an overdetermined (74 equations and 33 unknowns) linear adjustment process to solve for the heights. In this process, the updated surface normals are considered as the observations while the interpolated height values are the unknowns. This is simply done by approximating p and q with finite differences in terms of heights. The control goes back to the first step of this stage unless the average difference between the calculated and original image grey values of all the pixels in the patch is less than a predetermined threshold.

The last stage, postprocessing, consists of taking arithmetic means of two solutions for the unknown (interpolated) heights located on the boundary of the innermost square in each patches coming from the neighboring patches, except for the outsides of the peripheral patches.

3.2 Experimental Tests

In order to check the validity of the methodologies explained in Sections 2 and 3, a number of numerical examples using both simulated and real world data set are used. The following subsections describe the test procedures in more detail.

3.2.1 Simulated Data Set: First, one synthetic object and its corresponding synthetic imagery are created. The synthetic object is a 1024 by 1024 pixel convex hemisphere with a radius of 250 units, sampled at each 0.5 unit. The corresponding DTM (one dyadic order less than the object, i.e., 512 by 512 pixels) is extracted out of the object. Meanwhile, its corresponding image is created using a Lambertian reflectance model with a much denser version of the object while the albedo coefficient is set to 255. Then the grey level of each pixel is scaled to one of the randomly selected different levels trying to simulate the Earth surface with three different types of coverage .

The differences between the original object, the Interpolated Grid Solution (IGS) and the three SFS solutions, each in turn, in three different cases are analysed. In the first case (Table 3), the assumption is that the albedo coefficient is the same for all the pixels, i.e., same coverage type everywhere, and therefore no classification is done. In the second case, the Mahalanobis classifier with three different classes is used to classify the image pixels. 100 pixels for each class are used as the training data set. Once the pixels are assigned to a class, the average grey value of each class is used as the albedo coefficient for any pixel in that class. In the third case, using the interpolated height values and albedo of 255 for all the pixels, the image of each patch is reconstructed and is compared to the corresponding grey values in the original image file. The mean difference between these two grey values is used to scale the assumed albedo. Table 3 shows the percentages of the improvements in accuracy of DTM densification resulting from these analyses.

	Case 1	Case 2	Case 3
SFS1 vs IGS	18.2%	38.2%	20.5%
SFS2 vs IGS	23.2%	41.8%	26.2%
SFS3 vs IGS	25.6%	42.1%	28.7%

Table 3. Improvement percentages relative to corresponding IGS. Cases 1, 2, 3 show the No Classification, Classification with Mahalanobis classifier and Patchwise Classification cases respectively.

3.2.1   Real Data Set: The second object is a real terrain data set from southern Alberta (Waterton), Canada with 25 metre spacing in UTM coordinate system. A set of 1024 by 1024 grid with over 1300 metre height differences is selected from the four quadrants of NTS 82H04 DTM provincial data file. The originally measured DTM data consists of 100 metre spacing grid in addition to the feature points. These measurements had been used to interpolate the provincial 25-metre and other DTM grids.

The corresponding satellite imagery is a three channel SPOT data file with 20 metre resolution which was originally georeferenced to an extended UTM coordinate system. By extracting the coordinates of the predominant terrain features from the corresponding 1/20000 topographic map sheets, the SPOT imagery is georeferenced to the same coordinate system as the DTM data. For this purpose 23 points with good

distribution in the area under investigation are used. A second order polynomial is used for the purpose of georeferencing. The RMS of georeferencing in easting and northing directions are 2.96 m and 1.40 m respectively.

Using PCI software (from PCI Geomatics Enterprises Inc.), a principal component transformation is applied and the first channel with 88.52% energy is selected for these experiments. Then the satellite imagery pixel size is changed from 20 m to 25 m using a bilinear interpolation method.

The efficiency of the SFS methods with the real data set is analysed by trying to reconstruct the 25 m DTM from 50 m DTM and 25 m SPOT imagery. Similar to the simulated data case, the differences between the original object, the Interpolated Grid Solution (IGS) and the three SFS solutions each in turn in three different cases are analysed. In the first case, the assumption is that the albedo coefficient is the same for all the pixels, i.e., same coverage type everywhere, and therefore no classification is done. In the second case, the Mahalanobis classifier with the assumption of three different classes (water, soil and vegetation) is used to classify the image pixels. In doing that all the information in three channels of satellite imagery is used. 100 pixels for each class are used as the training data set. Once the pixels are assigned to their corresponding class, the average grey value of each class in the principal component transformed file is used as the albedo coefficient for any pixel in that class. In the third case, using the interpolated height values and albedo of 255 for all the pixels, the image of each patch is reconstructed and compared to the corresponding grey values in the principal component transformed file. The mean difference between these two grey values is used to scale the assumed albedo. Table 4 shows the results of these analyses.

	Case 1	Case 2	Case 3
SFS1 vs IGS	32.3%	42.2%	46.3%
SFS2 vs IGS	41.1%	48.6%	54.7%
SFS3 vs IGS	47.8%	51.4%	57.2%

Table 4. Improvement percentages relative to corresponding IGS. Cases 1, 2, 3 show the No Classification, Classification with Mahalanobis classifier and Patchwise Classification cases respectively.

4. CONCLUDING REMARKS

The experimental results in Tables 3 and 4 have been analysed and it is concluded that:

1. In all of these cases, applying any of the SFS methods will give us a more accurate densified DTM than the interpolation method. However, the percentage of improvement is different in each case. Generally speaking, it is seen that using a SFS method based on the curvature index will result in a better solution in comparison to the other SFS methods in the same case.

2. It is realized that the improvement percentages in the SFS solutions are higher with the real data set. That seems to imply that our simulated image generation was not as realistic as could be expected.

3. Applying classification methods to calibrate the albedo coefficient in the image irradiance model seems to improve

the SFS solutions. However, in case of simulated data set, the Mahalanobis classifier works better than the pacthwise classifier. There seem to be two main reasons for this. First, in the simulation process, the differences between albedo coefficients of different surface types were deliberately considered high. Then it is obvious that Mahalanobis classifier can classify the pixels with better accuracy in comparison to the real data case. Second, the distribution of pixels from different classes in the simulated image is too random to be compatible with the real data set. In other words, in simulating the image with different surface coverages, no correlation between neighboring pixels is considered which is not the case in reality. This seems to imply that patchwise interpolation is not appropriate for these simulated data sets.

4. Patchwise classification works better with the real data set case than the Mahalanobis classifier. This might be because of insufficient number of training data sets or inappropriate assumed numbers of classes. Having access to a land use map or other source of information such as aerial photography of the region can improve the classification quality in this case. Moreover, each patch in our case study is just an area of 150 m by 150 m which can easily satisfy the assumption of having the same ground type in the patch.

Based on the results of these experiments, future work will include:

1. Studying the behaviour of SFS techniques with different terrain types and DTM resolutions as well as satellite imageries of different quality.

2. As the SFS solutions used in these experiments are apparently suffering from over simplified irradiance models, more sophisticated image formation equations should be more deeply investigated especially for satellite imageries.

3. The terrain properties in the statistical analysis results shown here are assumed to be homogeneous and stationary. However, these assumptions are not true in reality. Obviously, domain segmentation is required and has to be taken into consideration. It goes without saying that the effectiveness of the SFS method in densifying DTM should be studied in rough terrain applications.

4. Each scene of satellite imagery usually covers a wide area of the Earth and the resolution can be as high as one metre or less. When dealing with such applications, tremendous amounts of computations have to be expected. Using parallel processing techniques in these types of applications is a must for general implementations.

5. REFERENCES

Brooks, M.J., Horn, B.K.P., 1985. Shape and Source from Shading. International Joint Conference on Artificial Intelligence, pp. 932-936.

Gugan, D.J., Dowman, I.J., 1988. Topographic Mapping from Spot Imagery. Photgrammetric Engineering and Remote Sensing 54(10), pp. 1409-1414.

Gultekin, A., Gokmen, M., 1996. Adaptive Shape From Shading. ISCIS XI The Eleventh International Symposium on Computer and Information Sciences, pp. 83-92.

Horn, B.K.P., 1970. Shape from Shading: A method for Obtaining the Shape of a Smooth Opaque from One View. Ph.D. Thesis, Massachusetts Ins. of Technology.

Horn, B.K.P., 1990. Height and gradient from shading. Int. J. Comput. Vision, 37-5.

Horn, B.K.P., 1990. Height and Gradient from Shading. Int. J. Comput. Vision , Vol. 5, No. 1, pp. 37-75.

Ikeuchi, K., Horn, B. K. P., 1981. Numerical Shape from Shading and Occluding Boundaries. Artificial Intelligence, Vol. 17, Nos. 1-3, pp. 141-184.

Koenderink, J.J., van Doorn, A., 1992. Surface Shape and Curvature Scales. Image and Vision Computing, Vol. 10, No. 8, October, pp. 557-565.

Rajabi, M.A., Blais, J.A.R., 2001. Densification of Digital Terrain Model Using Shape From Shading with Single Satellite Imagery. Lecture Notes in Computer Science, Vol. 2074, Springer, pp. 3-12.

Richards, J.A., 1986. *Remote Sensing Digital Analysis An Introduction.* Springer-Verlag, Berlin Heidelberg, pp.185-186

Simard, R., Rochon, G., Leclerc, A., 1988. Mapping with SPOT Imagery and Integrated Data Sets. Invited paper presented at the 16th congress of the International Society for Photogrammetry and Remote Sensing held July 1988 in Kyoto, Japan.

Tam, A.P., 1990. Terrain Information Extraction from Digital SPOT Satellite Imagery. Dept. of Geomatics Eng., The University of Calgary.

Worthington, P.L., Hancock, E.R., 1999. Needle Map Recovery Using Robust Regularizers. Image and Vision Computing, Vol. 17, pp. 545-557.

Zhang, R., Tsai, P.S., Cryer, J.E., Shah, M., 1994. Analysis of Shape from Shading Techniques. Proc. Computer Vision Pattern Recognition, pp. 377-384.

Zhang, R., Tsai, P.S., Cryer, J.E., Shah, M., 1999. Shape from Shading: A Survey. IEEE Transaction on Pattern Analysis and Machine Intelligence, Vol. 21, No. 8, August, pp. 690-706.